A statistical study of plasma sheet electrons carrying auroral upward field-aligned currents measured by Time History of Events and Macroscale Interactions during Substorms (THEMIS)

S. Lee,[1] K. Shiokawa,[1] J. P. McFadden,[2] and Y. Nishimura[1,3]

Received 22 June 2011; revised 23 September 2011; accepted 23 September 2011; published 2 December 2011.

[1] We have statistically investigated the electron density $n_{e,M}$ and temperature $T_{e,M}$ in the near-Earth plasma sheet in terms of the magnetosphere-ionosphere coupling process, as measured by the electrostatic analyzer (ESA) on board the Time History of Events and Macroscale Interactions during Substorms (THEMIS-D) satellite from November 2007 to January 2010. To find out when and where an aurora can occur, either with or without electron acceleration, the thermal current $j_{\parallel}^{th}$ and the conductivity K along the magnetic field line were also estimated from observations of the magnetospheric electrons with pitch angle information inside 12 R_E. The thermal current, $j_{\parallel}^{th}(\propto n_{e,M}\, T_{e,M}^{1/2})$, represents the upper limit of the field-aligned current that can be carried by magnetospheric electrons without a field-aligned potential difference. The conductivity, $K(\propto n_{e,M}\, T_{e,M}^{-1/2})$, relates the upward field-aligned current, $j_{\parallel}$, to the field-aligned potential difference, $V_{\parallel}$, assuming adiabatic electron transport. The thermal current is estimated by two methods: (1) from the relation by using $n_{e,M}$ and $T_{e,M}$ and (2) from the total downward electron number flux. We find that in the dawnside inner magnetosphere, the thermal currents estimated by both methods are sufficient to carry typical region 2 upward field-aligned current. On the other hand, in the duskside outer magnetosphere, a field-aligned potential difference is necessary on the region 1 current since the estimated thermal current is smaller than the typical region 1 current. By using the relationship, $j_{\parallel} = KV_{\parallel}$, where K is the conductivity estimated from Knight's relation and $j_{\parallel}$ is the typical auroral current, we conclude that a field-aligned potential difference of $V_{\parallel}$ = 2–5 kV is necessary on the duskside region 1 upward field-aligned current.

Citation: Lee, S., K. Shiokawa, J. P. McFadden, and Y. Nishimura (2011), A statistical study of plasma sheet electrons carrying auroral upward field-aligned currents measured by Time History of Events and Macroscale Interactions during Substorms (THEMIS), *J. Geophys. Res.*, *116*, A12202, doi:10.1029/2011JA016954.

1. Introduction

[2] Many recent studies have strived to understand auroral electron acceleration, because it provides vital insight into magnetosphere-ionosphere coupling processes along auroral field lines. Auroral structures are categorized into two primary types: discrete and diffuse aurora [*Davis*, 1978]. Discrete aurora, which has intense and bright features, is usually associated with downward electron acceleration along the magnetic field line above the ionosphere [*Frank and Ackerson*, 1971]. Diffuse aurora, which mostly shows temporal pulsation, is caused by precipitation of magnetospheric electrons without field-aligned electron acceleration. *Swift* [1981] reviewed the precipitations of different types of aurora: the diffuse aurora usually forms at the equatorward boundary of the auroral oval and the auroral patches and pulsations appear most commonly within the morning sector of the diffuse aurora; the discrete aurora is most prominently observed in the evening and poleward sectors of the auroral oval, and the "inverted-V" aurora appears in the same regions as discrete aurora but with much larger size scales. However, the mechanism that creates such different characteristics of aurora in latitudes and local times has not been clearly explained. Corresponding structures have not been identified in the magnetosphere.

[3] In the magnetosphere-ionosphere coupling system, field-aligned currents play a key role in the exchange of information between the two altitudes. In the ideal magnetohydrodynamic equations, field-aligned currents can be driven by magnetospheric processes, such as flow shear and azimuthal pressure gradients [*Hasegawa*, 1979; *Haerendel*, 1990]. For the ionosphere, *Knight* [1973] introduced the

[1]Solar-Terrestrial Environment Laboratory, Nagoya University, Nagoya, Japan.
[2]Space Sciences Laboratory, University of California, Berkeley, California, USA.
[3]Department of Atmospheric and Ocean Sciences, University of California, Los Angeles, California, USA.

0148-0227/11/2011JA016954

field-aligned current density, $j_{\parallel}$, carried by magnetospheric electrons accelerated along field lines

$$j_{\parallel} = en_{e,M}\left(\frac{\kappa T_{e,M}}{2\pi m_e}\right)^{1/2}\left(\frac{B_I}{B_M}\right)\left[1 - \left(1 - \frac{B_M}{B_I}\right)\exp\left(-\frac{eV_{\parallel}}{\kappa T_{e,M}\left(\frac{B_I}{B_M} - 1\right)}\right)\right] \quad (1)$$

where e, κ, and m_e are the electron charge, Boltzmann constant, and electron mass, respectively. $V_{\parallel}$ is a field-aligned potential difference that accelerates electrons downward. B_I and B_M are the magnetic field intensities in the ionosphere and in the source magnetosphere, respectively. Equation (1) is obtained by integrating the electron flux in the loss cone within the magnetosphere, assuming a Maxwellian distribution function for the magnetospheric electrons with density $n_{e,M}$ and temperature $T_{e,M}$. However, effects from backscattered electrons and pitch angle anisotropy for the magnetospheric plasma are ignored.

[4] In the case that no field-aligned potential difference exists (i.e., $V_{\parallel} = 0$), (1) is reduced to

$$j_{\parallel}^{th} = en_{e,M}\left(\frac{\kappa T_{e,M}}{2\pi m_e}\right)^{1/2}, \quad (2)$$

where $j_{\parallel}^{th}$ is the thermal current and represents the field-aligned current carried by magnetospheric electrons without field-aligned acceleration.

[5] In contrast, when $1 \ll eV_{\parallel}/\kappa T_{e,M} \ll B_I/B_M$, which is typical for auroral electrons acceleration, (1) then becomes [*Lyons*, 1980]

$$j_{\parallel} = KV_{\parallel}, \quad (3)$$

where

$$K = \frac{e^2 n_{e,M}}{\left(2\pi m_e \kappa T_{e,M}\right)^{1/2}}. \quad (4)$$

K, which is the conductivity, represents the efficiency of the upward field-aligned current, $j_{\parallel}$, that a field-aligned potential difference $V_{\parallel}$ can produce. Note that $j_{\parallel}^{th}$ and K depend only on the magnetospheric electron density $n_{e,M}$ and temperature $T_{e,M}$. Estimating $j_{\parallel}^{th}$ and K in the plasma sheet is important for understanding the ability of plasma sheet electrons to carry field-aligned current.

[6] When field-aligned current is conserved along a field line, the upward field-aligned current is carried by downgoing magnetospheric electrons, while the ionospheric ions are usually either gravitationally bound or, in the case of heated conics, have too small a flux to represent significant current. If $j_{\parallel}^{th}$, as expressed by equation (2), is enough to carry the field-aligned current driven by magnetospheric processes, then a field-aligned potential difference $V_{\parallel}$ is not necessary. If $j_{\parallel}^{th}$ is smaller than the driven current, then $V_{\parallel}$ needs to be formed. Thus, by estimating $j_{\parallel}^{th}$, and comparing it with typical auroral field-aligned current, one can estimate where, when, and how much $V_{\parallel}$ is necessary in the magnetosphere-ionosphere coupling system.

[7] *Shiokawa et al.* [2000] performed a similar study. They estimated $j_{\parallel}^{th}$ and K on the basis of auroral electron data obtained by the Active Magnetospheric Particle Tracer Explorers/Ion Release Module (AMPTE/IRM) satellite in the near-Earth plasma sheet at 10–18 R_E in February–June 1985 and March–June 1986, during the solar minimum. The results were compared with those from Defense Meteorological Satellite Program (DMSP) satellites above the auroral oval at an altitude of ~800 km. However, electron data for the inner magnetosphere (within 10 R_E) were not investigated. Moreover, pitch angle information for the electrons was missing from their data.

[8] In the present study, we statistically investigate the electron density $n_{e,M}$, temperature $T_{e,M}$, thermal current $j_{\parallel}^{th}$, and conductivity K in the plasma sheet within 12 R_E with pitch angle information. To do this, we used electron spectra obtained by probe 3 (THEMIS-D) of the Time History of Events and Macroscale Interactions during Substorms (THEMIS) satellite over 2.25 years, during the solar minimum of 2007–2010. From this investigation, it is suggested that a field-aligned potential difference is particularly necessary for the dusk region 1 upward field-aligned current, where $j_{\parallel}^{th}$ is not sufficient to carry the typical current.

2. Data

[9] The THEMIS spacecrafts, launched on 17 February 2007, are equipped with comprehensive in situ particle and field instruments that measure thermal and superthermal ions and electrons [*Angelopoulos*, 2008]. For the present analysis, the following data from onboard THEMIS instruments are used: electron data for energies from a few electron volts up to 30 keV, as measured by an electrostatic analyzer (ESA) [*McFadden et al.*, 2008]; magnetic field data obtained by a flux gate magnetometer (FGM) [*Auster et al.*, 2008]; and spacecraft potential data from an electric field instrument (EFI) [*Bonnell et al.*, 2008]. THEMIS consists of five probes, named THEMIS-B (probe 1), THEMIS-C (probe 2), THEMIS-D (probe 3), THEMIS-E (probe 4), and THEMIS-A (probe 5). Since we intend to investigate within 12 R_E, we select the THEMIS-D probe, which orbits in a near-equatorial plane with an apogee of ~12 R_E and a perigee of ~2 R_E.

[10] Figure 1 shows an example of the 1 day summary plot from THEMIS-D on 15 December 2008. From top to bottom, Figure 1 shows the three components (Bx, By, and Bz) of magnetic field in GSM coordinates (Figure 1a), densities (Figure 1b) and temperatures (Figure 1c) of both electrons (red) and ions (black), the three components (Vx, Vy, and Vz) of ion velocity in GSM coordinates (Figure 1d), omnidirectional ion energy-time spectra (Figure 1e), omnidirectional electron energy-time spectra, with the satellite potential represented by the black line (Figure 1f), and thermal currents, $j_{\parallel}^{th}$ (Figure 1g). THEMIS-D passed the inner radiation belt at the perigee (with $X_{GSM} = 0.12$ R_E, $Y_{GSM} = 1.6$ R_E) at dusk at 0028 UT, and outer magnetosphere at the apogee (with $X_{GSM} = -0.7$ R_E, $Y_{GSM} = -11.53$ R_E) at dawn at 1227 UT.

[11] The plasma sheet electron data used in the present analysis were acquired during the time interval between the two vertical lines A and B in Figure 1. The plasma sheet is identified using the following features.

[12] 1. THEMIS-D occasionally detects magnetosheath particles. Therefore, by checking for electron data with high density (>10 cm^{-3}) and low temperature (<100 eV), and for

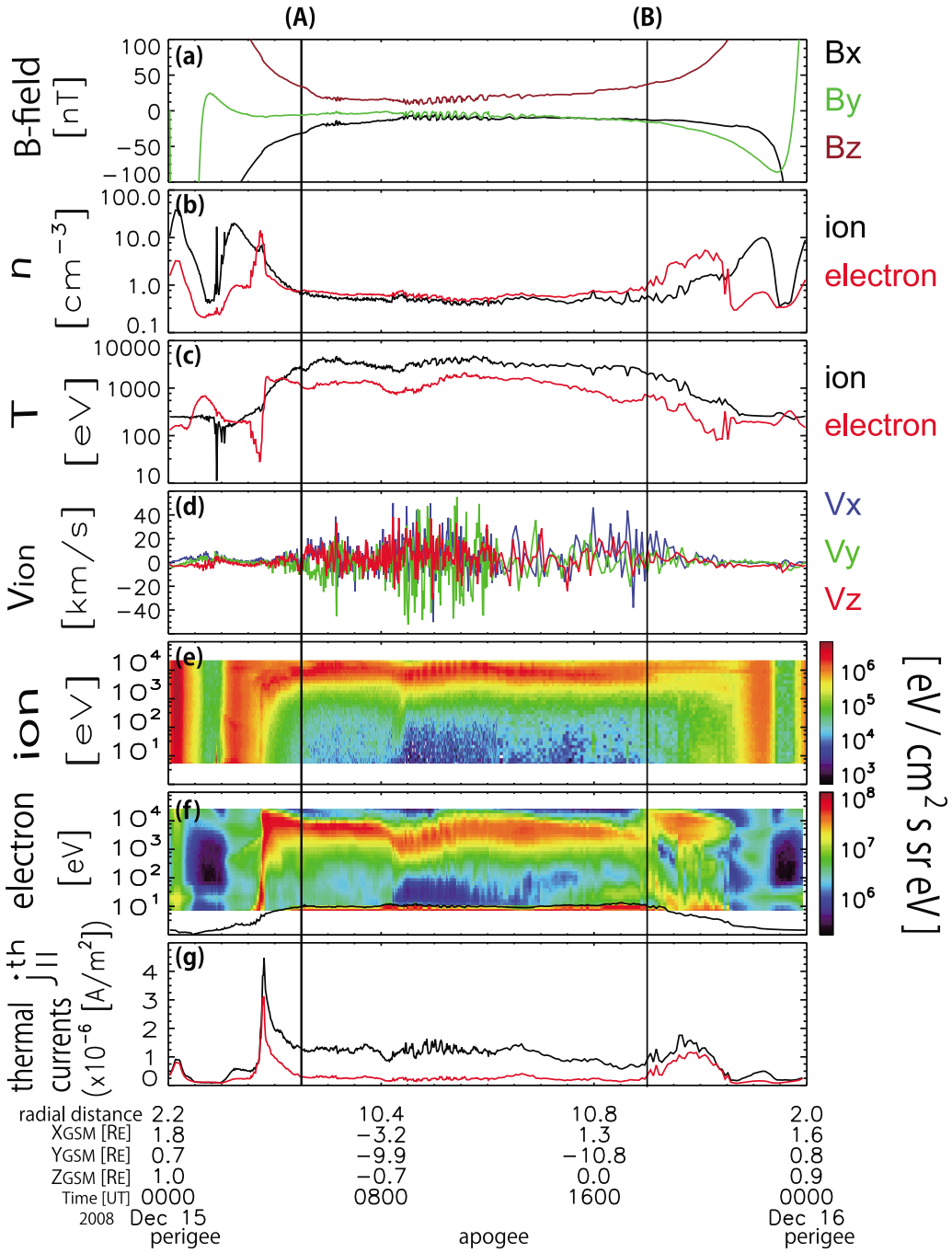

Figure 1. Example of the 1 day summary plots, taken from THEMIS-D on 15 December 2008. (a) The three components (Bx, By, and Bz) of the magnetic field in GSM coordinates, (b) densities and (c) temperatures of both the electrons (red lines) and ions (black lines), (d) the three components (Vx, Vy, and Vz) of the ion velocity in GSM coordinates, (e) omnidirectional ion energy-time spectra, (f) omnidirectional electron energy-time spectra, with the satellite potential represented by the black line, and (g) thermal currents $j_{\parallel}^{th}$, estimated with (red line) and without (black line) assuming a Maxwellian distribution. The interval between lines A and B indicates the plasma sheet defined in this study.

electron energy-time spectra with high fluxes at low energies (<1000 eV), data were excluded when THEMIS-D goes out of the magnetopause.

[13] 2. To avoid radiation belt particles in the inner magnetosphere, we use the data outside 7 R_E.

[14] 3. Within the plasma sheet, the densities of the electrons and ions have approximately the same values as shown in Figure 1b, whereas they are significantly different in the radiation belt, as shown outside the time interval A–B.

[15] 4. The densities of both the electrons and ions start to increase rapidly as the satellite approaches the radiation belt.

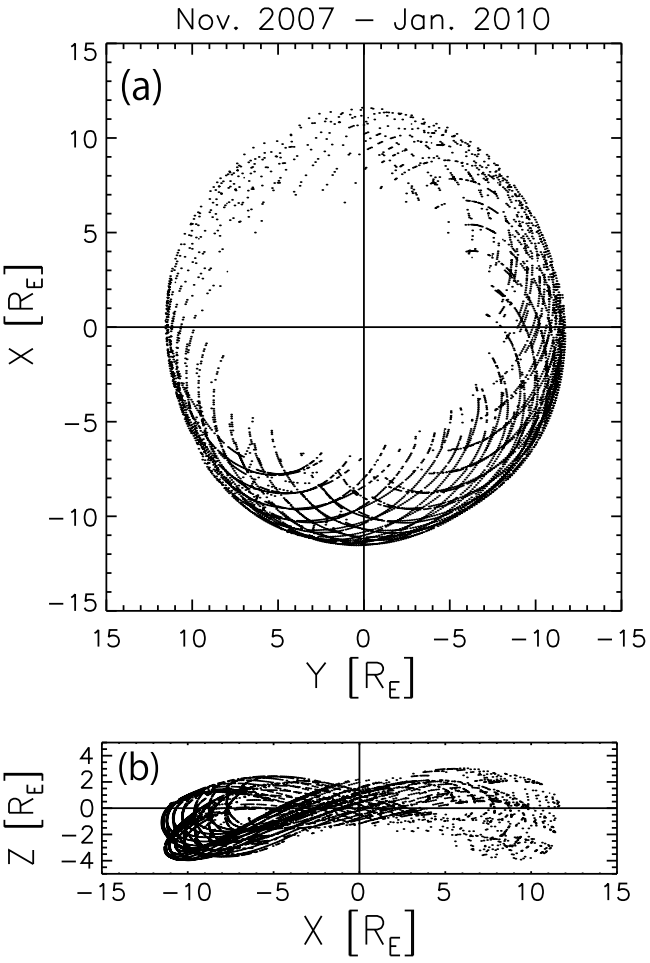

Figure 2. THEMIS-D plasma sheet orbits from 1 November 2007 to 31 January 2010, defined as the plasma sheet in this study, in (a) X_{GSM}-Y_{GSM} coordinates and (b) Z_{GSM}-X_{GSM} coordinates. Each point indicates a trace for each day.

[16] 5. The characteristics of the energy spectrograms in Figure 1f are also considered in order to identify the plasma sheet, in which the electron and ion spectra tend to show high fluxes at high energies.

[17] In estimating the electron density, temperature, and flux, we do not subtract the background counts due to contamination with high-energy particles because either they are negligible in the plasma sheet or in most cases they do not affect flux. From the satellite potential data, obtained by using a single-probe measurement, electron data below the satellite potential are excluded, since they are contaminated by photoelectrons. The satellite potential gradually increases from the inner magnetosphere to the outer magnetosphere and correlates well with the upper boundary of the high-flux, low-energy electrons seen in the spectrograms in Figure 1f. Since we used equations (1)–(4) in the analysis, we assumed that the auroral electrons follow the adiabatic theory and come from the equatorial plasma sheet to the ionosphere.

[18] Figure 2 shows the orbits of THEMIS-D after exclusion of the radiation belts in the inner magnetosphere and the magnetosheath outside the magnetopause. The orbits are given in GSM coordinates. It is clearly seen that the selected THEMIS-D orbits cover from 7 to 12 R_E and the equatorial plane in $|Z_{GSM}| < 5$ R_E over all local times.

[19] The average electron density $n_{e,M}$ is shown in Figure 3 in terms of magnetic local time (MLT). In Figures 3a and 3b the average electron densities are plotted for the daytime (9–15 MLT) and nighttime (21–3 MLT) during magnetically quiet periods when AE < 100 nT (Figure 3a), and for active times when AE > 100 nT (Figure 3b). Densities at dawn (3–9 MLT) and dusk (15–21 MLT) are plotted similarly in Figures 3c and 3d for quiet and active times, respectively. The solid and dashed lines in Figure 3 correspond to the pitch angles of the electron data, where pitch angles between 0° and 30° are defined as "quasi-parallel" and those between 60° and 90° are defined as "perpendicular." The term quasi-parallel is used because the loss cone cannot be resolved, and the parallel distribution is approximated by assuming that its angle range has similar values to the pitch angle scattered population. Finally, the thick and thin lines in Figure 3 represent the different MLTs and the error bars indicate $\pm 0.2\sigma$. Because the number of events is very small at 7–8 R_E during the daytime and at dusk during the magnetically active time, these values are not plotted. The densities are generally higher during the nighttime than during the daytime, and higher at dawn than at dusk during both the quiet and active times. Additionally, densities increase with decreasing radial distance for all local times, and values at small radial distances are higher during magnetically active times than during quiet times. Moreover, the densities of quasi-parallel electrons are higher than those of perpendicular electrons during the nighttime and at dusk.

[20] The average electron temperatures, $T_{e,M}$, shown in Figure 4, are plotted in the same format as Figure 3. Figure 4 shows that temperatures are generally higher during the nighttime than during the daytime and higher at dawn than at dusk. This is especially true within 10 R_E, for both magnetically quiet and active times. It can also be seen that temperatures tend to decrease with decreasing radial distance inside 10 R_E for all local times, except for at dawn during active times. In addition, temperatures are higher during magnetically active times than during quiet times, and temperatures are clearly higher for perpendicular than for quasi-parallel electrons.

[21] The average thermal currents $j_{\parallel}^{th}$ shown in Figure 5 are plotted in the same format as Figures 3 and 4. It is observed that the thermal currents during the nighttime and at dawn are higher than those during the daytime and at dusk, respectively, since the thermal current is proportional to both the density and square root of the temperature. For similar reasons, the thermal currents tend to increase with decreasing radial distance for all local times, both magnetically quiet and active, except at dawnside during quiet times and at duskside during active times, which tend to decrease within 9–10 R_E. Furthermore, at dawn, during the active time, the thermal current increases significantly with decreasing radial distance. At large radial distances, the thermal currents during quiet times are comparable with those during active times; however, at small radial distances, the thermal currents during active times are much larger than those during quiet times. During the nighttime, the thermal

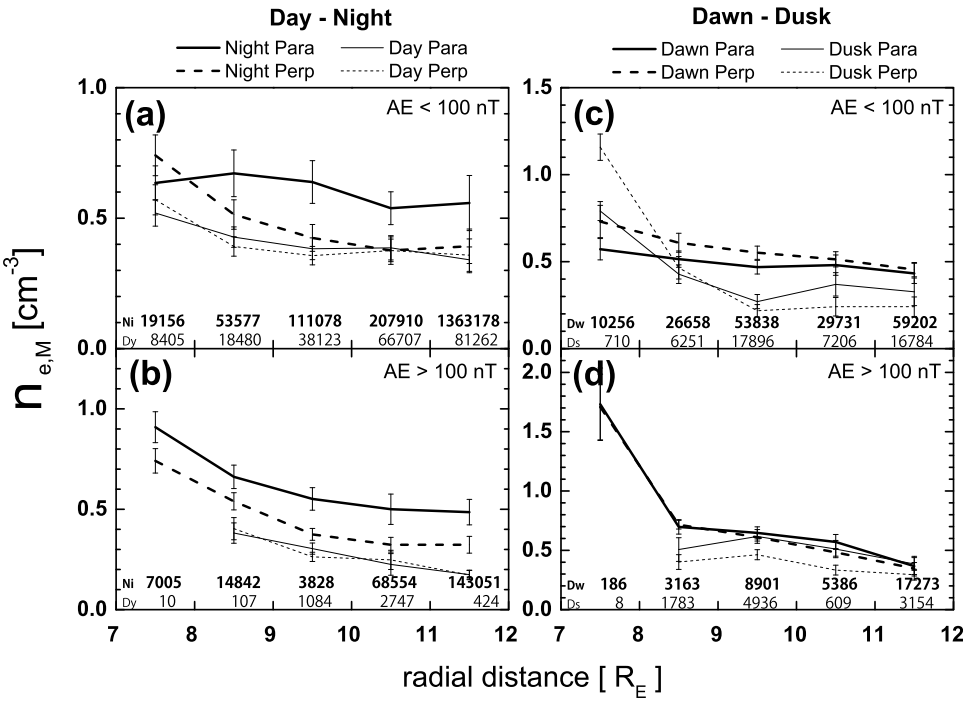

Figure 3. Average electron density, $n_{e,M}$, in terms of magnetic local times (MLTs). During the daytime (9–15 MLT) and nighttime (21–3 MLT), $n_{e,M}$ is found during the (a) magnetically quiet time (AE < 100 nT) and (b) active time (AE > 100 nT). Similarly, the density is found at dawn (3–9 MLT) and dusk (15–21 MLT) during the (c) quiet and (d) active times. The solid and dashed lines represent the pitch angles of electrons, where pitch angles of 0°–30° are defined as quasi-parallel (Para) and 60°–90° as perpendicular (Perp). Thick and thin lines represent different MLTs, and error bars indicate $\pm 0.2\sigma$. The numbers of data points are shown at the bottom of each panel. Since the number of events is very small between 7 and 8 R_E during the daytime and at dusk in the active times, these values are not plotted.

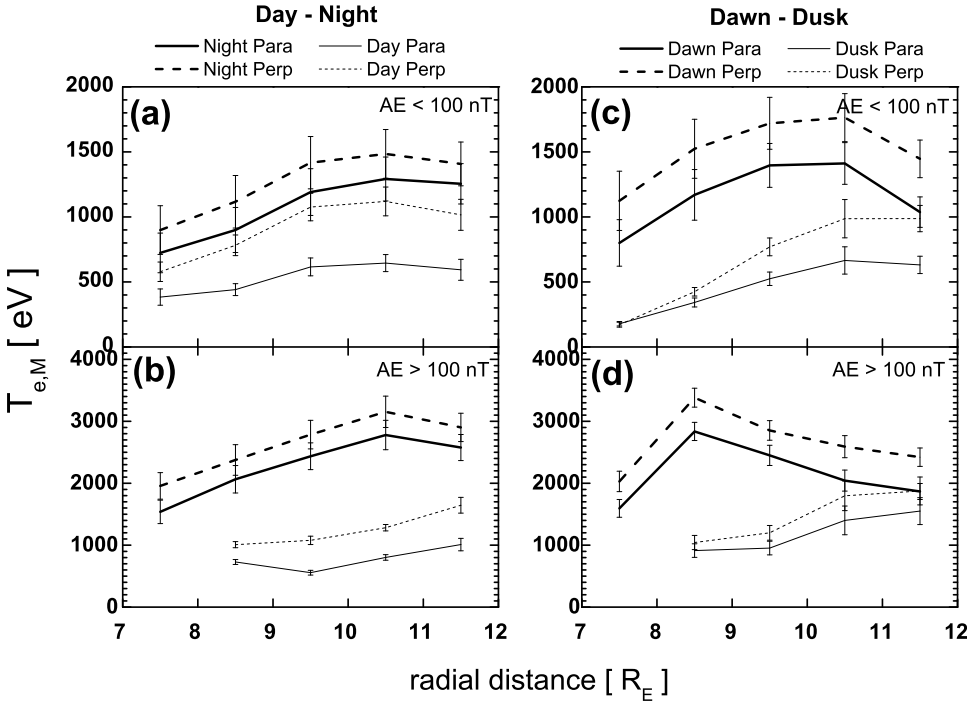

Figure 4. Average electron temperatures, $T_{e,M}$, plotted using the same format as Figure 3.

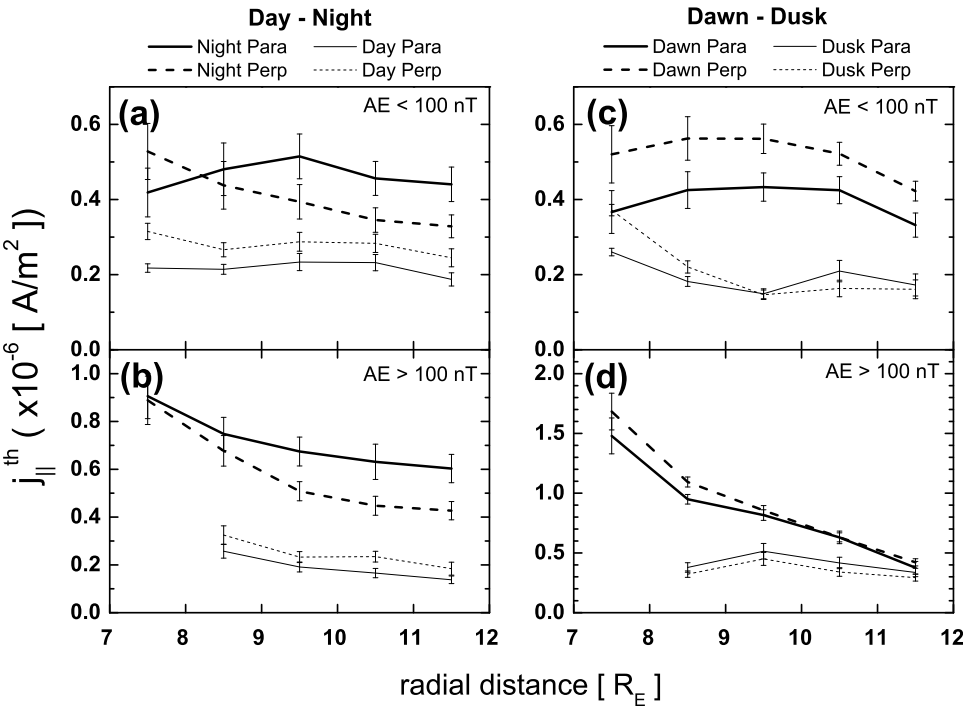

Figure 5. Average thermal currents, $j_{||}^{th}$, estimated from inputting values of $n_{e,M}$ and $T_{e,M}$ into equation (2) and plotted using the same format as Figure 3.

currents estimated from quasi-parallel electron data are, in general, higher than perpendicular thermal currents during both quiet and active times, as well as at dusk during active times, whereas the perpendicular thermal currents are higher than the quasi-parallel ones during the daytime and at dawn, throughout both quiet and active times.

[22] Last, the average conductivities K are presented in Figure 6 in the same format as Figures 3–5. It is found that

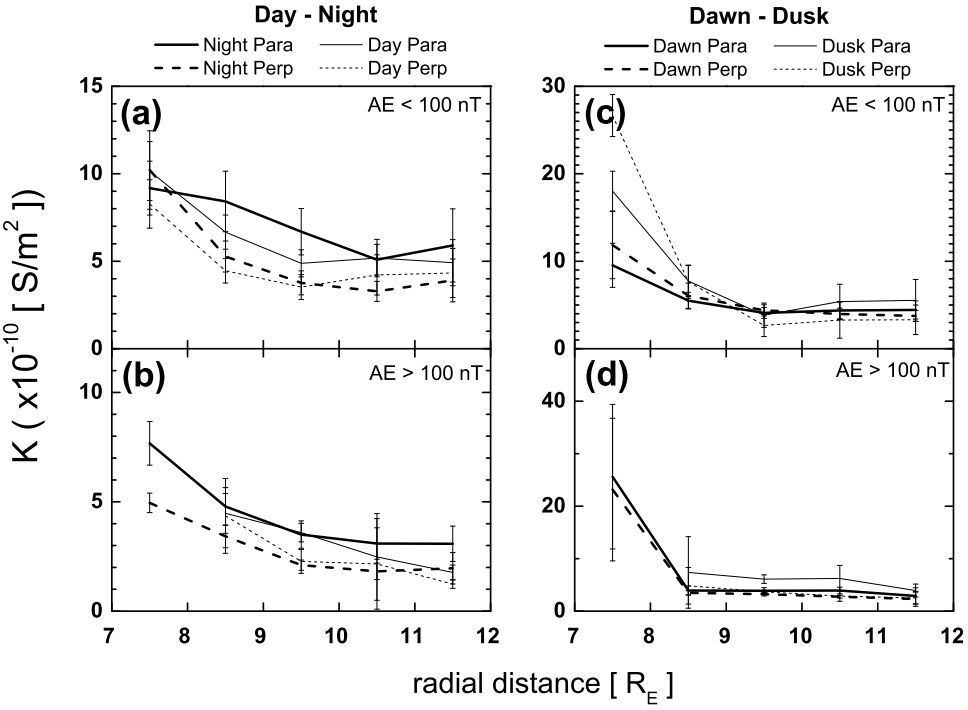

Figure 6. Average conductivities, K, estimated by inputting values for $n_{e,M}$ and $T_{e,M}$ into (4) and plotted using the same format as Figure 3.

Table 1. Averages of the Electron Density $n_{e,M}$, Temperature $T_{e,M}$, Thermal Current $j_{\parallel}^{th}$, and Conductivity K, for the Inner Magnetosphere (7–9 R_E) at Dawn

	Quasi-parallel		Perpendicular	
Parameter	AE > 100 nT	AE < 100 nT	AE > 100 nT	AE < 100 nT
Density $n_{e,M}$ (cm^{-3})	0.6–1.7	0.4–0.6	0.6–1.7	0.5–0.7
Temperature $T_{e,M}$ (eV)	1500–2500	800–1400	2000–3500	1100–1700
Thermal current $j_{\parallel}^{th}$($\mu A/m^2$)	0.8–1.5	0.3–0.5	0.8–1.7	0.5–0.6
Conductivity K (10^{-10} S/m^2)	3–25	4–10	3–23	4–12

the conductivities tend to increase with decreasing radial distance and that the conductivities estimated by using quasi-parallel electron data are generally higher than perpendicular conductivities, especially outside 9 R_E.

3. Discussion

[23] First, let us discuss where and when a potential difference would be formed by comparing the present results with observations for the field-aligned current found previously by *Iijima and Potemra* [1976], who presented a polar map for the field-aligned current distribution determined from magnetic field measurements made by the Triad satellite during the period from July 1973 to October 1974. Region 1 field-aligned currents, located at a higher latitude of the auroral oval, consist of an upward current at dusk and a downward current at dawn. Conversely, region 2 field-aligned currents, located at a lower latitude, consist of a downward current at dusk and upward current at dawn. By considering typical magnetic field configurations, the magnetospheric source region of duskside region 1 and dawnside region 2 upward currents would be connected to the dusk plasma sheet outside of 10 R_E and dawn plasma sheet inside of 10 R_E, respectively. *Iijima and Potemra* [1976] reported that the duskside region 1 upward current and dawnside region 2 upward current have values of 1.0–1.4 $\mu A/m^2$ and 0.4–0.6 $\mu A/m^2$, respectively, for magnetically quiet times (Kp = 1–3), and 1.5–2.0 $\mu A/m^2$ and 0.7–0.8 $\mu A/m^2$ for active times (Kp = 3–5).

[24] For comparison with the results found here, values of $n_{e,M}$, $T_{e,M}$, $j_{\parallel}^{th}$, and K in these two source regions (dawnside at radial distances of 7–9 R_E and duskside at 9–12 R_E) for both magnetically active and quiet times, including quasi-parallel and perpendicular pitch angles, are summarized in Tables 1 and 2. From Table 1, at dawn at radial distances of 7–9 R_E during magnetically quiet times (AE < 100 nT), the density, temperature, and thermal current for the quasi-parallel electrons are 0.4–0.6 cm^{-3}, 800–1400 eV, and 0.3–0.5 $\mu A/m^2$, respectively. It is thus seen that the thermal current is comparable with typical region 2 upward field-aligned currents (0.4–0.6 $\mu A/m^2$). From Table 1, during the magnetically active time (AE > 100 nT), the density, temperature, and thermal current for the quasi-parallel electrons are 0.6–1.7 cm^{-3}, 1500–2500 eV, and 0.8–1.5 $\mu A/m^2$, respectively. The thermal current is comparable to, or higher than, typical region 2 upward field-aligned currents (0.7–0.8 $\mu A/m^2$) observed in the ionosphere. Hence, magnetospheric electrons are able to carry sufficient currents for region 2 upward current without field-aligned acceleration.

[25] Precipitation without acceleration is caused by electrons in the loss cone, which has a very small pitch angle (<1.0°). For electrons to be precipitated into the ionosphere continuously, the loss cone needs to be continuously refilled with electrons from outside the loss cone. Precipitation of auroral electrons can occur by particle scattering into the loss cone through wave-particle interactions [*Tsurutani and Lakhina*, 1997].

[26] From Table 2, at dusk at radial distances of 9–12 R_E during magnetically quiet times (AE < 100 nT), the quasi-parallel density, temperature, and thermal current are 0.2–0.3 cm^{-3}, 500–700 eV, and 0.1–0.2 $\mu A/m^2$, respectively. Hence, the thermal currents are clearly lower than typical region 1 upward field-aligned currents (1.0–1.4 $\mu A/m^2$). During active times (AE > 100 nT), the quasi-parallel densities, temperatures, and the thermal currents are 0.3–0.6 cm^{-3}, 900–1500 eV, and 0.3–0.5 $\mu A/m^2$, respectively. The thermal currents are again smaller than typical region 1 upward field-aligned currents (1.5–2.0 $\mu A/m^2$). Since the estimated thermal currents are not sufficient for typical region 1 current for both quiet and active times, auroral electron acceleration would be necessary in this region. Thus, field-aligned potential difference is expected for the dusk region 1 current, but not for the dawn region 2 current. A field-aligned potential difference would be distributed along the field line, particularly at low altitudes near the ionosphere, to satisfy the quasi-neutrality condition, as discussed in detail by *Lennartsson* [1977], *Chiu and Schulz* [1978], and *Stern* [1981].

Table 2. Averages of Electron Density $n_{e,M}$, Temperature $T_{e,M}$, Thermal Current $j_{\parallel}^{th}$, and Conductivity K for the Outer Magnetosphere (9–12 R_E) at Dusk

	Quasi-parallel		Perpendicular	
Parameter	AE > 100 nT	AE < 100 nT	AE > 100 nT	AE < 100 nT
Density $n_{e,M}$ (cm^{-3})	0.3–0.6	0.2–0.3	0.2–0.5	0.2–0.3
Temperature $T_{e,M}$ (eV)	900–1500	500–700	1000–2000	700–1000
Thermal current $j_{\parallel}^{th}$ ($\mu A/m^2$)	0.3–0.5	0.1–0.2	0.3–0.5	0.1–0.2
Conductivity K (10^{-10} S/m^2)	4–7	3–6	2–4	2–3

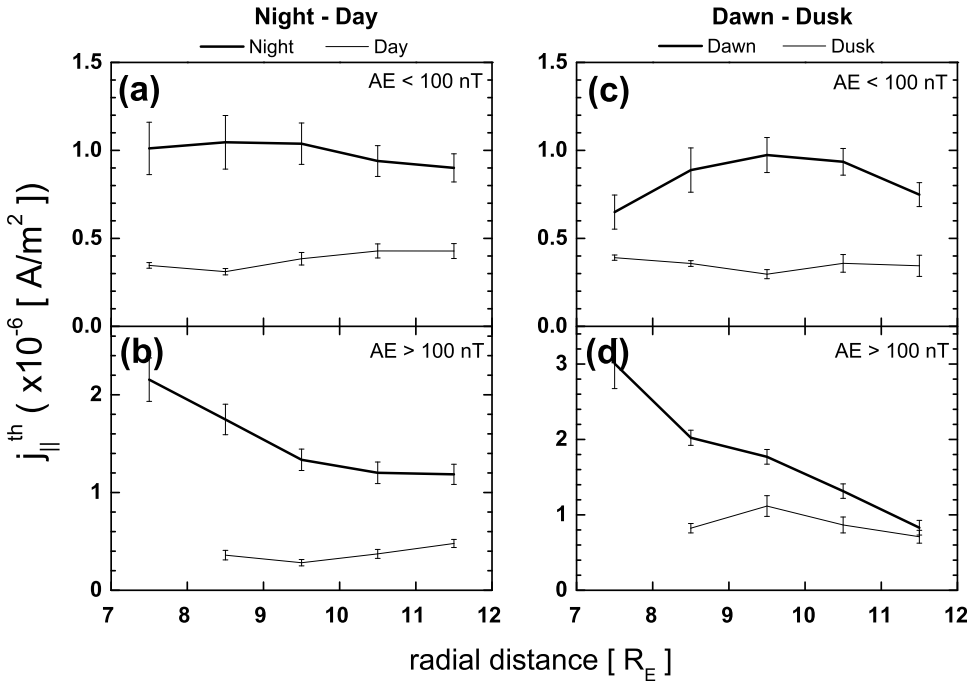

Figure 7. Average thermal currents, $j_{\parallel}^{th}$, estimated from the total downward electron number flux and plotted using the same format as Figure 3.

[27] We should address the source region for the dusk region 1 upward field-aligned current, which is assumed to be located at 9–12 R_E in the present study. This source region could extend beyond the THEMIS-D orbit coverage of 12 R_E, since region 1 currents extend to the poleward boundary of the auroral oval, where the field line connects to the mid or distant tail. The results in Figures 3 and 5 show that as duskside densities tend to decrease with increasing radial distance, the associated thermal current also decreases with distance. Taking this tendency into account, the thermal current outside 12 R_E would probably decrease with increasing radial distance. Thus, our conclusion that the thermal current is smaller than typical region 1 current is not changed even outside 12 R_E.

[28] That the field-aligned acceleration is necessary for the dusk region 1 upward current is consistent with the statistical distribution of a field-aligned potential difference shown by *Newell et al.* [1996]. They reported a high probability of observing electron acceleration at dusk on the basis of a large set of data on precipitating electrons, as measured by DMSP satellites from December 1983 to November 1992.

[29] Note that although Knight's relationship in equation (1) used for the present study assumes a Maxwellian distribution for plasma sheet electrons, actual plasma sheet electrons mostly do not follow a single Maxwellian distribution. Therefore, we also estimate the thermal current without the assumption of a Maxwellian distribution. This estimation is achieved by integrating the observed electron spectra to obtain the total downward electron number flux, which represents the electron flux that can reach the ionosphere and, hence, is equal to $j_{\parallel}^{th}/e$. Figure 1g shows example of these two thermal currents for the 1 day summary plot. The red line indicates the thermal current calculated from equation (2), and the black line indicates the thermal current found from the total electron number flux without the assumption of a Maxwellian distribution. The thermal current obtained from the total number flux is generally higher than that from equation (2), which is derived from Knight's relation, by a factor of 2–3. The accuracy of Knight's relation has been controversial. *Morooka et al.* [2004] discussed that the current estimated from Knight's relation might be underestimated if the electrons at source region do not have an isotropic Maxwellian distribution function. *Fridman and Lemaire* [1980] introduced the formula assuming bi-Maxwellian distribution for the primary electrons in the source region.

[30] Figure 7 shows the statistical average thermal currents, obtained from the total electron number flux without the Maxwellian distribution assumption, for quiet (AE < 100 nT) and active (AE > 100 nT) magnetic local times. Note that the scale on the vertical axis is different in each plot. It can be observed that the thermal currents at magnetically quiet times (Figures 7a and 7c) are smaller than those at active times (Figures 7b and 7d). For obvious reasons, a dawn-dusk asymmetry exists during both quiet and active times. Further, the thermal currents are smaller at dawn than during the nighttime in the magnetically quiet period, while the thermal currents are higher at dawn than during the nighttime in the active period. At dawn inside 9 R_E during active times, the thermal currents are 2.0–3.0 μA/m^2, much larger than typical dawnside region 2 currents of 0.7–0.8 μA/m^2. On the other hand, at dusk outside 9 R_E during active times, the thermal currents are 0.7–1.1 μA/m^2, smaller than typical duskside region 1 currents of 1.5–2.0 μA/m^2. Although from Figure 7 the thermal currents obtained by using the total flux are 2 times higher than those calculated from equation (2), it is again concluded that a field-aligned potential difference is necessary for the dusk

region 1 upward field-aligned current, and not necessary for the dawn region 2 upward field-aligned current.

[31] From equation (3), the potential difference $V_{\parallel}$ is equal to $j_{\parallel}/K$. Thus we can estimate how much a potential difference is needed between the magnetosphere and ionosphere. Note that the conductivity K was obtained from equation (4). The conductivity estimated using the formula by *Fridman and Lemaire* [1980] with assumption of bi-Maxwellian distribution is roughly 0.7–0.9 times smaller than that using Knight's relation with isotropic Maxwellian assumption of equation (4). Using the typical dusk region 1 auroral current given by *Iijima and Potemra* [1976] stated as 1.5–2.0 μA/m^2, and a value for the conductivity of 4–7 $\times$ 10^{-10} S/m^2 given in Table 2 from our observations, an average field-aligned potential difference of $V_{\parallel}$ = 2–5 kV is estimated for the duskside region 1 upward field-aligned current. Although we assumed the adiabatic transport of the magnetospheric electrons to estimate the field-aligned potential difference, the estimated potential difference is well consistent with those reported by other researchers using ionospheric satellite data [e.g., *Burch et al.*, 1976; *Bosqued et al.*, 1986; *Reiff et al.*, 1988; *Shiokawa and Fukunishi*, 1991; *Marklund et al.*, 2011]. Recently, a statistical study by *Partamies et al.* [2008] using a huge number of inverted-V events observed by Fast Auroral Snapshot (FAST) from 1997 to 2001 showed that the typical maximum energies of the inverted-V events are 2–4 keV, mainly less than 6 keV.

[32] However, the region 1 and 2 currents reported by *Iijima and Potemra* [1976] are large-scale field-aligned currents, whereas actual field-aligned currents usually have many complicated small-scale structures. Individual small-scale currents, such as those corresponding to individual inverted-V events, can be higher than the large-scale currents [e.g., *Hoffman et al.*, 1985; *Bosqued et al.*, 1986]. Therefore, a field-aligned potential difference associated with a small-scale acceleration event would be larger than the 2–5 kV estimated above. We should also note that we did not consider the electron acceleration processes by dispersive Alfvén wave, which are quite localized and highly variable. Several observations showed that such processes provide significant contributions to auroral particle acceleration, using Freja satellite [e.g., *Andersson et al.*, 2002], FAST satellite [e.g., *Ergun et al.*, 2005; *Chaston et al.*, 2007], and Polar satellite [*Wygant et al.*, 2002; *Dombeck et al.*, 2005]. In this study, however, it is difficult to distinguish small-scale electron acceleration by dispersive Alfvén waves using the magnetospheric satellite.

[33] It should be also noted that we considered that the downward electrons from equatorial plasma sheet are the carriers responsible for the upward field-aligned current. Using the Akebono satellite data, *Sakanoi et al.* [1995] showed that the conductivities estimated from the potential drops and field-aligned current densities using the relation $j_{\parallel} = KV_{\parallel}$ is 2–20 times larger than those calculated from Knight's relation using source electron density and temperature obtained by fitting accelerated Maxwellian function. They suggested that the upward field-aligned current in the inverted-V region is significantly carried by low-energy electrons such as secondary and backscattered ionospheric electrons through nonadiabatic transport across magnetic field line. *Morooka et al.* [2004] showed using the Akebono satellite data that the low-energy electrons often play an important role as additional current carriers in the middle altitude of the particle acceleration region, where the parallel electric fields exist above and below the observation point, while the high-energy primary electrons are accelerated adiabatically. However, the Akebono measurements with a time resolution of 8 s might average over the edges of auroral arcs where Knight's relation may not apply. Using the FAST satellite data with much higher time resolutions of 13–78 ms, *McFadden et al.* [1999a, 1999b] discussed that regions of low-density cavities are shown to contain little or no cold plasma, but rather only hot plasma that is consistent with Knight's relation in those cases where the magnetospheric population is a single Maxwellian. We estimated that field-aligned potential difference is 2–5 kV by using $V_{\parallel} = j_{\parallel}/K$, where K is calculated using Knight's relation. These values of 2–5 kV applies to the center of arcs, which is the only place where Knight's relation applies, and are well consistent with previous observations. From this consideration, we speculate that the general feature of large-scale field-aligned potential differences and associated upward field-aligned currents might be explained by the adiabatic electrons in the equatorial plasma sheet, while the small-scale structures of potential difference and upward field-aligned current might be controlled by nonadiabatic mechanisms such as wave-particle interaction for low-energy electrons near the edges of auroral arcs.

[34] By comparing the electron densities and temperatures of equatorial plasma sheet with those estimated by fitting accelerated Maxwellian distribution for inverted-V events, *Shiokawa et al.* [2000] suggested that the source region of inverted-V electrons might be just above the acceleration region. The conductivities estimated by *Sakanoi et al.* [1995] using Knight's relation might imply electron densities and temperatures at middle altitudes. The conductivities in our study were estimated from the electron density and temperature of equatorial plasma sheet. We speculate that the upward field-aligned currents are carried away from the equatorial plasma sheet up to near the acceleration region by downward high-energy plasma sheet electrons. Because of mirroring effect of downward electrons, the flux from the plasma sheet does not fully reach the ionosphere, as described by Knight's relation. The role of low-energy electrons may therefore become important to keep carrying the upward field-aligned currents near the acceleration region. *Chiu and Schulz* [1978] indicated from one-dimensional model calculations by considering the mirroring effect and quasi-neutrality with ambient plasma that the resultant potential difference tends to be formed at lower altitudes below 10,000 km.

[35] To understand the differences between current and previous results, values for $n_{e,M}$, $T_{e,m}$, $j_{\parallel}^{th}$, and K obtained in the present study are compared in Table 3 with those from the AMPTE/IRM satellite, given by *Shiokawa et al.* [2000]. These parameters, averaged over all pitch angles and all MLTs, are shown at the radial distance of 9–12 R_E for our study and 9–19 R_E for the data of *Shiokawa et al.* [2000]. Both sets of data were obtained during solar minimum periods. The densities and temperatures measured by the two satellites during magnetically quiet time and the densities during active time are similar, while the temperatures measured by THEMIS during magnetically active time are slightly higher than those measured by AMPTE/IRM. This

Table 3. Comparison Between the Averages for Electron Density $n_{e,M}$, Temperature $T_{e,M}$, Thermal Current $j_{\parallel}^{th}$, and Conductivity K Obtained at 9–12 R_E by the THEMIS-D and at 9–19 R_E by AMPTE/IRM Satellites[a]

	THEMIS-D		AMPTE/IRM	
	AE > 100 nT	AE < 100 nT	AE > 100 nT	AE < 100 nT
Density $n_{e,M}$ (cm^{-3})	0.3–0.5	0.4–0.5	0.3–0.4	0.4–0.5
Temperature $T_{e,M}$ (eV)	1000–1500	300–600	600–800	200–500
Thermal current $j_{\parallel}^{th}$ ($\mu A/m^2$)	0.3–0.5	0.2–0.3	0.2–0.3	0.1–0.2
Conductivity K (10^{-10} S/m^2)	2–3	4–5	3–5	6–10

[a]See *Shiokawa et al.* [2000].

might be due to the difference of radial distances. According to Figure 3 of *Shiokawa et al.* [2000], electron density and temperature decrease with increasing radial distances. Another possibility might be the difference of actual magnetic activity defined by AE > 100 nT. According to Figure 4 of *Shiokawa et al.* [2000], temperature increases and density decreases with increasing AE index. With the different radial distances, if the magnetic activity level in the present study is higher than that in the study by *Shiokawa et al.* [2000], the temperatures by THEMIS might be higher than those by AMPTE/IRM and the densities by two satellites might be comparable. However, we do not know the average AE index in the study by *Shiokawa et al.*, [2000]. The thermal currents and conductivities estimated from THEMIS are about 1.5–2 times higher and lower than those estimated from AMPTE/IRM, respectively, because of these differences in density and temperature.

[36] As for the pitch angle dependence shown in Figure 3, the densities, $n_{e,M}$, of quasi-parallel electrons are higher than those of perpendicular electrons both at night and at dusk during quiet and active times for all MLTs. The temperatures of quasi-parallel electrons are lower than those of perpendicular electrons, as shown in Figure 4. A possible origin of these features is the upward ionospheric electrons, which have much higher densities and lower temperatures than plasma sheet electrons. The upgoing electrons from the ionosphere become field-aligned parallel electrons in the magnetosphere.

[37] Another possible reason for the high temperatures of perpendicular electrons is due to perpendicular Betatron acceleration of these electrons. *Hada et al.* [1981] and *Shiokawa et al.* [2003] showed that the occurrence rate for bidirectional parallel electrons in the plasma sheet increases during magnetically active times, and suggested that this was a result of Fermi acceleration of parallel electrons in the plasma sheet. In contrast, the average perpendicular temperatures during both active and quiet times are higher than the quasi-parallel temperature in our observations. This fact indicates that perpendicular Betatron acceleration may be more effective than parallel Fermi acceleration within the plasma sheet. According to *Sharber and Heikkila* [1972], Betatron acceleration is responsible on the dipolar field lines near the Earth (<∼10 R_E), whereas Fermi acceleration predominates on the distant tail-like field lines (>∼10 R_E), under the adiabatic invariance. The radial distance of our study is from 7 to 12 R_E that is relatively closer to the Earth.

[38] Finally, we note that we assume isotropic distribution in 30° angle range. This definition is necessary for the statistical analysis, though the field-of-view of the ESA telescope is about 22°. As shown in Figure 3, it looks that the densities show isotropic distribution except for the night side, while the temperatures show unisotropic distribution. But these anisotropies are between quasi-parallel and quasi-perpendicular direction. Further detailed investigation would be necessary for the electron pitch angle distribution inside the 30°, particularly near the loss cone.

4. Conclusions

[39] The magnetospheric electron density, temperature, thermal current, and field-aligned conductivity have been statistically investigated, on the basis of measurements taken by the THEMIS-D satellite from November 2007 to January 2010. With the thermal current being the amount of upward field-aligned current that can be carried by downgoing magnetospheric electrons without field-aligned electron acceleration, the thermal current was estimated from equation (2) by inputting the electron density and temperature and assuming a Maxwellian electron distribution function and from the total downward electron number flux, obtained by integrating the observed electron spectra. The conclusions from this investigation are summarized as follows:

[40] 1. On the dawnside at 7–9 R_E, which is the source of region 2 upward current, the thermal currents estimated by the two methods are comparable to, or higher than, typical auroral current during both magnetically quiet and active times. As a result, a field-aligned potential difference is not necessary for the region 2 upward current.

[41] 2. On the duskside at 9–12 R_E, which is the source of region 1 upward current, the thermal currents estimated by the two methods are smaller than typical auroral current during both quiet and active times. Therefore, field-aligned potential difference is needed for the region 1 upward current.

[42] 3. From the relationship $j_{\parallel} = KV_{\parallel}$, where field-aligned conductivity K is estimated by using Knight's relation, a field-aligned potential difference of 2–5 kV is expected for the region 1 upward field-aligned current at dusk.

[43] 4. For the pitch angle dependence, quasi-parallel electron densities tend to be higher during the nighttime and at dusk, and the quasi-parallel temperatures are lower than those for the perpendicular electrons at all local times. This fact indicates a contribution from upward ionospheric electrons with high densities and low temperatures in the parallel direction. The high temperatures of the perpendicular electrons suggest that Betatron acceleration is more effective than Fermi acceleration in the magnetosphere.

[44] **Acknowledgements.** This work was supported by the Global COE Program of Nagoya University, "Quest for Fundamental Principles in the Universe (QFPU)," and by Grants-in-Aid for Scientific Research

(19403010, 20244080, and 23403009) from JSPS and MEXT of Japan. We acknowledge NASA contract NAS5-02099 and V. Angelopoulos for use of data from the THEMIS mission. Specifically, K. H. Glassmeier, U. Auster, and W. Baumjohann are acknowledged for the use of FGM data provided under the lead of the Technical University of Braunschweig and with financial support through the German Ministry for Economy and Technology and the German Center for Aviation and Space (DLR), under contract 50OC 0302. We also acknowledge J. W. Bonnell and F. S. Mozer for permitting the use of the EFI data.

[45] Robert Lysak thanks the reviewers for their assistance in evaluating this paper.

References

Andersson, L., N. Ivchenko, J. Clemmons, A. A. Namgaladze, B. Gustavsson, J.-E. Wahlund, L. Eliasson, and R. Y. Yurik (2002), Electron signatures and Alfvén waves, *J. Geophys. Res.*, *107*(A9), 1244, doi:10.1029/2001JA900096.

Angelopoulos, V. (2008), The THEMIS mission, *Space Sci. Rev.*, *141*, 5–34.

Auster, H. U., et al. (2008), The THEMIS fluxgate magnetometer, *Space Sci. Rev.*, *141*, 235–264.

Bonnell, J. W., F. S. Mozer, G. T. Delory, A. J. Hull, R. E. Ergun, C. M. Cully, V. Angelopoulos, and P. R. Harvey (2008), The electric field instrument (EFI) for THEMIS. *Space Sci. Rev.*, *141*, 303–341.

Bosqued, J. M., C. Maurel, J. A. Sauvaud, R. A. Kovrazhkin, and Y. I. Galperin (1986), Observations of auroral electron inverted-V structures by the AUREOL-3 satellite, *Planet. Space Sci.*, *34*, 255–269.

Burch, J. L., S. A. Fields, W. B. Hanson, R. A. Heelis, R. A. Hoffman, and R. W. Janetzke (1976), Characteristics of auroral electron acceleration regions observed by Atmosphere Explorer C, *J. Geophys. Res.*, *81*, 2223–2230.

Chaston, C. C., C. W. Carlson, J. P. McFadden, R. E. Ergun, and R. J. Strangeway (2007), How important are dispersive Alfvén waves for auroral particle acceleration?, *Geophys. Res. Lett.*, *34*, L07101, doi:10.1029/2006GL029144.

Chiu, Y. T., and M. Schulz (1978), Self-consistent particle and parallel electrostatic field distributions in the magnetospheric-ionospheric auroral region, *J. Geophys. Res.*, *83*, 629–642.

Davis, T. N. (1978), Observed characteristics of auroral forms, *Space Sci. Rev.*, *22*, 77–113.

Dombeck, J., C. Cattell, J. R. Wygant, A. Keiling, and J. Scudder (2005), Alfvén waves and Poynting flux observed simultaneously by Polar and FAST in the plasma sheet boundary layer, *J. Geophys. Res.*, *110*, A12S90, doi:10.1029/2005JA011269.

Ergun, R. E., L. Andersson, Y.-J. Su, D. L. Newman, M. V. Goldman, W. Lotko, C. C. Chaston, and C. W. Carlson (2005), Localized parallel electric fields associated with inertial Alfvén waves, *Phys. Plasmas*, *12*, 072901.

Frank, L. A., and K. L. Ackerson (1971), Observations of charged particle precipitation into the auroral zone, *J. Geophys. Res.*, *76*, 3612–3643.

Fridman, M., and J. Lemaire (1980), Relationship between auroral electrons fluxes and field aligned electric potential difference, *J. Geophys. Res.*, *85*, 664–670.

Hada, T., A. Nishida, T. Terasawa, and E. W. Hones Jr. (1981), Bi-directional electron pitch angle anisotropy in the plasma sheet, *J. Geophys. Res.*, *86*, 11,211–11,224.

Haerendel, G. (1990), Field-aligned currents in the Earth's magnetosphere, in *Physics of Magnetic Flux Ropes*, *Geophys. Monogr. Ser.*, vol. 58, edited by C. R. Russell, E. R. Priest, and L. C. Lee, pp. 539–553, AGU, Washington, D. C.

Hasegawa, A. (1979), Generation of field aligned current during substorm, in *Dynamics of the Magnetosphere*, edited by S.-I. Akasofu, pp. 529–542, D. Reidel, Norwell, Mass.

Hoffman, R. A., M. Sugiura, and N. C. Maynard (1985), Current carriers for the field-aligned current system, *Adv. Space. Res.*, *5*, 109–126.

Iijima, T., and T. A. Potemra (1976), The amplitude distribution of field-aligned currents at northern high latitudes observed by Triad, *J. Geophys. Res.*, *81*, 2165–2174.

Knight, S. (1973), Parallel electric fields, *Planet. Space Sci.*, *21*, 741–750.

Lennartsson, W. (1977), On high-latitude convection field inhomogeneities, parallel electric fields and inverted-V precipitation events, *Planet. Space Sci.*, *25*, 89–101.

Lyons, L. R. (1980), Generation of large-scale regions of auroral currents, electric potentials, and precipitation by the divergence of the convection electric field, *J. Geophys. Res.*, *85*, 17–24.

Marklund, G. T., S. Sadeghi, T. Karlsson, P.-A. Lindqvist, H. Nilsson, C. Forsyth, A. Fazakerley, E. A. Lucek, and J. Pickett (2011), Altitude distribution of the auroral acceleration potential determined from cluster satellite data at different heights, *Phys. Rev. Lett.*, *106*, 055002.

McFadden, J. P., C. W. Carlson, and R. E. Ergun (1999a), Microstructure of the auroral acceleration region as observed by FAST, *J. Geophys. Res.*, *104*, 14,453–14,480.

McFadden, J. P., C. W. Carlson, R. E. Ergun, D. M. Klumpar, and E. Moebius (1999b), Ion and electron characteristics in auroral density cavities associated with ion beams: No evidence for cold ionospheric plasma, *J. Geophys. Res.*, *104*, 14,671–14,682.

McFadden, J. P., C. W. Carlson, D. Larson, M. Ludlam, R. Abiad, B. Elliott, P. Turin, M. Marckwordt, and V. Angelopoulos (2008), The THEMIS ESA plasma instrument and in-flight calibration, *Space Sci. Rev.*, *141*, 277–302.

Morooka, M., T. Mukai, and H. Fukunishi (2004), Current–voltage relationship in the auroral particle acceleration region, *Ann. Geophys.*, *22*, 3641–3655.

Newell, P. T., K. M. Lyons, and C. I. Meng (1996), A large survey of electron acceleration events, *J. Geophys. Res.*, *101*, 2599–2614.

Partamies, N., E. Donovan, and D. Knudsen (2008), Statistical study of inverted-V structrues in FAST data, *Ann. Geophys.*, *26*, 1439–1449.

Reiff, P. H., H. L. Collin, J. D. Craven, J. L. Burch, J. D. Winningham, E. G. Shelley, L. A. Frank, and M. A. Friedman (1988), Determination of auroral electrostatic potentials using high- and low-altitude particle distributions, *J. Geophys. Res.*, *93*, 7441–7465.

Sakanoi, T., H. Fukunishi, and T. Mukai (1995), Relationship between field-aligned currents and inverted-V parallel potential drops observed at midaltitudes, *J. Geophys. Res.*, *100*, 19,343-19,360.

Sharber, J. R., and W. J. Heikkila (1972), Fermi acceleration of auroral particles, *J. Geophys. Res.*, *77*, 3397–3410.

Shiokawa, K., and H. Fukunishi (1991), Global characteristics of field-aligned acceleration processes associated with auroral arcs, *J. Geomagn. Geoelectr.*, *43*, 691–719.

Shiokawa, K., W. Baumjohann, G. Haerendel, and H. Fukunishi (2000), High- and low-altitude observations of adiabatic parameters associated with auroral electron acceleration, *J. Geophys. Res.*, *105*, 2541–2550.

Shiokawa, K., W. Baumjohann, and G. Paschmann (2003), Bi-directional electrons in the near-Earth plasma sheet, *Ann. Geophys.*, *21*, 1497–1507.

Stern, D. P. (1981), One-dimensional models of quasi-neutral parallel electric fields, *J. Geophys. Res.*, *86*, 5839–5860.

Swift, D. W. (1981), Mechanisms for auroral precipitation: A review, *Rev. Geophys.*, *19*, 185–211.

Tsurutani, B. T., and G. S. Lakhina (1997), Some basic concepts of wave-particle interactions in collisionless plasmas, *Rev. Geophys.*, *35*, 491–502.

Wygant, J. R., et al. (2002), Evidence for kinetic Alfvén waves and parallel electron energization at 4–6 R_E altitudes in the plasma sheet boundary layer, *J. Geophys. Res.*, *107*(A8), 1201, doi:10.1029/2001JA900113.

S. Lee, Y. Nishimura, and K. Shiokawa, Solar-Terrestrial Environment Laboratory, Nagoya University, Furo-cho, Chikusa-ku, Nagoya, 464–8601, Japan. (selee@stelab.nagoya-u.ac.jp)

J. P. McFadden, Space Sciences Laboratory, University of California, Berkeley, CA 94720, USA.